Since January 2020 Elsevier has created a COVID-19 resource centre with free information in English and Mandarin on the novel coronavirus COVID-19. The COVID-19 resource centre is hosted on Elsevier Connect, the company's public news and information website.

Resource

Cell Host & Microbe

Neutralizing Antibody and Soluble ACE2 Inhibition of a Replication-Competent VSV-SARS-CoV-2 and a Clinical Isolate of SARS-CoV-2

Graphical Abstract

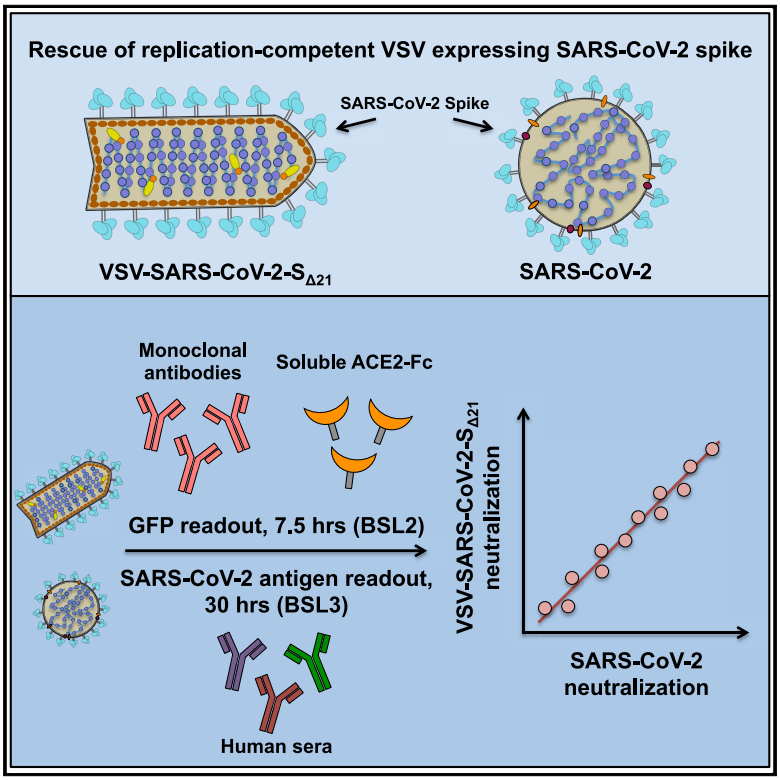

Highlights

- Vesicular stomatitis virus encoding the SARS-CoV-2 spike replicates to high titers
- Virus propagation is enhanced by a truncation in the cytoplasmic tail of the spike
- Neutralization can be assessed by BSL2 and BSL3 high-throughput assays
- SARS-CoV-2- and VSV-SARS-CoV-2-based neutralization assays correlate

Authors

James Brett Case, Paul W. Rothlauf, Rita E. Chen, ..., Daved H. Fremont, Michael S. Diamond, Sean P.J. Whelan

Correspondence

diamond@wusm.wustl.edu (M.S.D.), spjwhelan@wustl.edu (S.P.J.W.)

In Brief

Case, Rothlauf et al. generate a replication-competent vesicular stomatitis virus (VSV) expressing the SARS-CoV-2 spike and compare the neutralizing activity of antibodies with VSV-SARS-CoV-2 to fully infectious SARS-CoV-2. They show that VSV-SARS-CoV-2 is a useful BSL2 surrogate virus, as neutralization profiles strongly correlate with focus-reduction neutralization tests using SARS-CoV-2.

Case et al., 2020, Cell Host & Microbe *28*, 475–485
September 9, 2020
https://doi.org/10.1016/j.chom.2020.06.021

CellPress

Cell Host & Microbe

CellPress

Resource

Neutralizing Antibody and Soluble ACE2 Inhibition of a Replication-Competent VSV-SARS-CoV-2 and a Clinical Isolate of SARS-CoV-2

James Brett Case,[1,11] Paul W. Rothlauf,[2,6,11] Rita E. Chen,[1,3] Zhuoming Liu,[2] Haiyan Zhao,[3] Arthur S. Kim,[1,3] Louis-Marie Bloyet,[2] Qiru Zeng,[2] Stephen Tahan,[2] Lindsay Droit,[2] Ma. Xenia G. Ilagan,[4] Michael A. Tartell,[2,6] Gaya Amarasinghe,[2,3,4] Jeffrey P. Henderson,[1] Shane Miersch,[7] Mart Ustav,[7] Sachdev Sidhu,[7] Herbert W. Virgin,[8] David Wang,[2,3] Siyuan Ding,[2] Davide Corti,[9] Elitza S. Theel,[10] Daved H. Fremont,[2,3,4,5] Michael S. Diamond,[1,2,3,5,*] and Sean P.J. Whelan[2,12,*]

[1]Department of Medicine, Washington University School of Medicine, St. Louis, MO, USA
[2]Department of Molecular Microbiology, Washington University School of Medicine, St. Louis, MO, USA
[3]Department of Pathology & Immunology, Washington University School of Medicine, St. Louis, MO, USA
[4]Department of Biochemistry & Molecular Biophysics, Washington University School of Medicine, St. Louis, MO, USA
[5]The Andrew M. and Jane M. Bursky Center for Human Immunology & Immunotherapy Programs, Washington University School of Medicine, St. Louis, MO, USA
[6]Program in Virology, Harvard Medical School, Boston, MA, USA
[7]The Donnelly Centre, University of Toronto, Toronto, Canada
[8]Vir Biotechnology, San Francisco, CA, USA
[9]Humabs BioMed SA, a subsidiary of Vir Biotechnology, Inc., CH-6500, Bellinzona, Switzerland
[10]Division of Clinical Microbiology, Department of Laboratory Medicine and Pathology, Mayo Clinic, Rochester, MN, USA
[11]These authors contributed equally
[12]Lead Contact
*Correspondence: diamond@wusm.wustl.edu (M.S.D.), spjwhelan@wustl.edu (S.P.J.W.)
https://doi.org/10.1016/j.chom.2020.06.021

SUMMARY

Antibody-based interventions against SARS-CoV-2 could limit morbidity, mortality, and possibly transmission. An anticipated correlate of such countermeasures is the level of neutralizing antibodies against the SARS-CoV-2 spike protein, which engages with host ACE2 receptor for entry. Using an infectious molecular clone of vesicular stomatitis virus (VSV) expressing eGFP as a marker of infection, we replaced the glycoprotein gene (G) with the spike protein of SARS-CoV-2 (VSV-eGFP-SARS-CoV-2) and developed a high-throughput-imaging-based neutralization assay at biosafety level 2. We also developed a focus-reduction neutralization test with a clinical isolate of SARS-CoV-2 at biosafety level 3. Comparing the neutralizing activities of various antibodies and ACE2-Fc soluble decoy protein in both assays revealed a high degree of concordance. These assays will help define correlates of protection for antibody-based countermeasures and vaccines against SARS-CoV-2. Additionally, replication-competent VSV-eGFP-SARS-CoV-2 provides a tool for testing inhibitors of SARS-CoV-2 mediated entry under reduced biosafety containment.

INTRODUCTION

Severe acute respiratory syndrome coronavirus 2 (SARS-CoV-2) is a positive-sense, single-stranded, enveloped RNA virus that was first isolated in Wuhan, China in December, 2019 from a cluster of acute respiratory illness cases (Guan et al., 2020). SARS-CoV-2 is the etiologic agent of coronavirus disease 2019 (COVID-19), which as of June 17, 2020 has more than 8.2 million confirmed cases causing 445,000 deaths. Virtually all countries and territories have been affected, with major epidemics in Central China, Italy, Spain, France, Iran, Russia, Brazil, India, Peru, the United Kingdom, and the United States. SARS-CoV-2 is thought to be of zoonotic origin and is closely related to the original SARS-CoV (Zhang et al., 2020; Zhou et al., 2020). Most cases are spread by direct human-to-human transmission, with community transmission occurring from both symptomatic and asymptomatic individuals (Bai et al., 2020). This has resulted in a global pandemic with severe economic, political, and social consequences. The development, characterization, and deployment of an effective vaccine or antibody prophylaxis or treatment against SARS-CoV-2 could prevent morbidity and mortality and curtail its epidemic spread.

The viral spike protein (S) mediates all steps of coronavirus entry into target cells, including receptor binding and membrane fusion (Tortorici and Veesler, 2019). During viral biogenesis, the S protein undergoes furin-dependent proteolytic processing as it transits through the trans-Golgi network and is cleaved into S1 and S2 subunits that function in receptor binding and

membrane fusion, respectively (Walls et al., 2020). Angiotensin-converting enzyme 2 (ACE2) serves as a cell surface receptor (Letko et al., 2020; Wrapp et al., 2020) for SARS-CoV-2, and productive infection is facilitated by additional processing of S2 by the host cell serine protease TMPRSS2 (Hoffmann et al., 2020).

Laboratory studies of SARS-CoV-2 require biosafety level 3 (BSL3) containment with positive-pressure respirators. Single-round pseudotyped viruses complemented by expression of the SARS-CoV-2 S protein *in trans* serve as biosafety level 2 (BSL2) surrogates that can facilitate studies of viral entry and the inhibition of infection by neutralizing antibodies and other inhibitors (Hoffmann et al., 2020; Lei et al., 2020; Nie et al., 2020; Ou et al., 2020). Such pseudotyping approaches are used routinely by many laboratories for other highly pathogenic coronaviruses, including SARS-CoV and MERS-CoV (Fukushi et al., 2005, 2006; Giroglou et al., 2004; Kobinger et al., 2007). Viral pseudotyping assays are limited by the need to express the glycoprotein *in trans* and preclude forward genetic studies of the viral envelope protein. Expression of the glycoprotein is often accomplished by plasmid transfection, which requires optimization to minimize batch variation. Assays performed with such pseudotyped viruses rely on relative levels of infectivity as measured by a reporter assay without correlation to an infectious titer. It also is unknown how the display of S proteins on a heterologous virus impacts viral entry, antibody recognition, and antibody neutralization compared to infectious coronavirus. This question is important because neutralization assays are used to establish correlates of protection for vaccine and antibody-based countermeasures, and most manufacturers lack access to high-containment laboratories to test antibody responses against highly pathogenic coronaviruses such as SARS-CoV-2.

Here, we developed a simple and robust BSL2 assay for evaluating SARS-CoV-2 entry and its inhibition by antibodies. We engineered an infectious molecular clone of vesicular stomatitis virus (VSV) to encode the SARS-CoV-2 S protein in place of the native envelope glycoprotein (G) and rescued an autonomously replication-competent virus bearing the spike. Through passage of VSV-eGFP-SARS-CoV-2, we selected a gain-of-function mutation in S that allowed more efficient viral propagation yielding titers of $>1 \times 10^8$ plaque-forming units (PFU)/mL. We characterized this variant with respect to inhibition by soluble human ACE2-Fc and monoclonal and polyclonal antibodies from humans and compared those results to neutralization tests with a clinical isolate of SARS-CoV-2. These studies demonstrate that a recombinant VSV expressing SARS-CoV-2 S behaves analogously to a clinical isolate of SARS-CoV-2, providing a useful high-throughput BSL2 assay for studying antibody neutralization or inhibition of viral spike-mediated entry.

RESULTS

A Replication-Competent, Infectious VSV Chimera with SARS-CoV-2 S Protein

To generate a replication-competent virus to study entry and neutralization of SARS-CoV-2 at BSL2, we engineered an infectious molecular clone of VSV by replacing the endogenous glycoprotein (G) with SARS-CoV-2 S (Figure 1A). SARS-CoV-2 S protein contains an endoplasmic reticulum (ER) retention sequence in the cytoplasmic tail (KxHxx-COOH) because virion assembly occurs in ER-Golgi intermediate compartments (Lontok et al., 2004; McBride et al., 2007; Ruch and Machamer, 2012). We pre-emptively altered that sequence to AxAxx to facilitate retargeting of S to the plasma membrane, the site of VSV assembly. Using established approaches (Figure S1A) (Whelan et al., 1995), we recovered infectious VSV-eGFP-SARS-CoV-2-S_{AA} as determined by expression of the virus-encoded eGFP reporter (Figure 1A, right). However, VSV-eGFP-SARS-CoV-2-S_{AA} propagation was inefficient on Vero CCL81 cells. This result prompted us to test additional modifications of the cytoplasmic tail of S, which were also defective in autonomous amplification (Figure S1B). To overcome this limitation, we used a forward genetic approach to isolate two adaptive variants of VSV-eGFP-SARS-CoV-2-S_{AA} (Figure S1C). Virus was plaque-purified from the transfected cell supernatants, and one variant was passaged twice on Vero CCL81 cells. Following subsequent plaque isolation and serial amplification, we sequenced the viral RNA in infected cells at the seventh passage. A second, independent plaque from transfected cell supernatants was passaged an additional five times on a rhesus monkey MA104 cell line. Both approaches led to the emergence of a virus that contained a single mutation, a cysteine to stop mutation at residue 1253 (TGC to TGA at nucleotide 3759), which truncates the cytoplasmic tail of SARS-CoV-2 S by 21 residues (Figure 1A). This virus, hereafter referred to as VSV-SARS-CoV-2-$S_{\Delta 21}$, was passed 12 times in total to assess genetic stability by next generation sequencing, which revealed no additional mutations in the spike (SRA: SRR11878607; BioProject: PRJNA635934). Comparison of plaque morphology of VSV-SARS-CoV-2-$S_{\Delta 21}$ and VSV-eGFP-SARS-CoV-2-S_{AA} on three Vero cell subtypes and MA104 cells demonstrates that the selected variant spreads more efficiently (Figure 1B). Screening of a larger panel of cell types (Figure 1C) identified MA104 and Vero E6 cells as supporting the highest levels of virus production. Ectopic expression of TMPRSS2 led to a further ~10-fold increase in viral titer and larger plaque size (Figure 1D). VSV-SARS-CoV-2-$S_{\Delta 21}$ also was capable of infecting Calu-3 cells, a human epithelial lung adenocarcinoma cell line (Figure S2).

SARS-CoV-2-$S_{\Delta 21}$ Is Incorporated into Infectious VSV Particles

To confirm incorporation of SARS-CoV-2 S into particles, we first amplified the virus in the presence of VSV G to allow infection of cell types independently of the S protein. The VSV G *trans*-complemented VSV-SARS-CoV-2-$S_{\Delta 21}$ efficiently infects HEK293T cells, which then serve as a source of production of virus particles containing SARS-CoV-2 S protein. Western blotting of supernatants with CR3022, a cross-reactive anti-S monoclonal antibody (mAb) (ter Meulen et al., 2006; Yuan et al., 2020), established the presence of $S_{\Delta 21}$ in VSV-SARS-CoV-2-$S_{\Delta 21}$ particles, but not in the parental VSV (Figure 1E). The protein detected migrated at ~100 kilodaltons, a band that corresponds to the cleaved S1 subunit of the glycoprotein (Watanabe et al., 2020). To examine whether the $S_{\Delta 21}$ incorporated into VSV particles is processed to S1 and S2, we performed [^{35}S] cysteine-

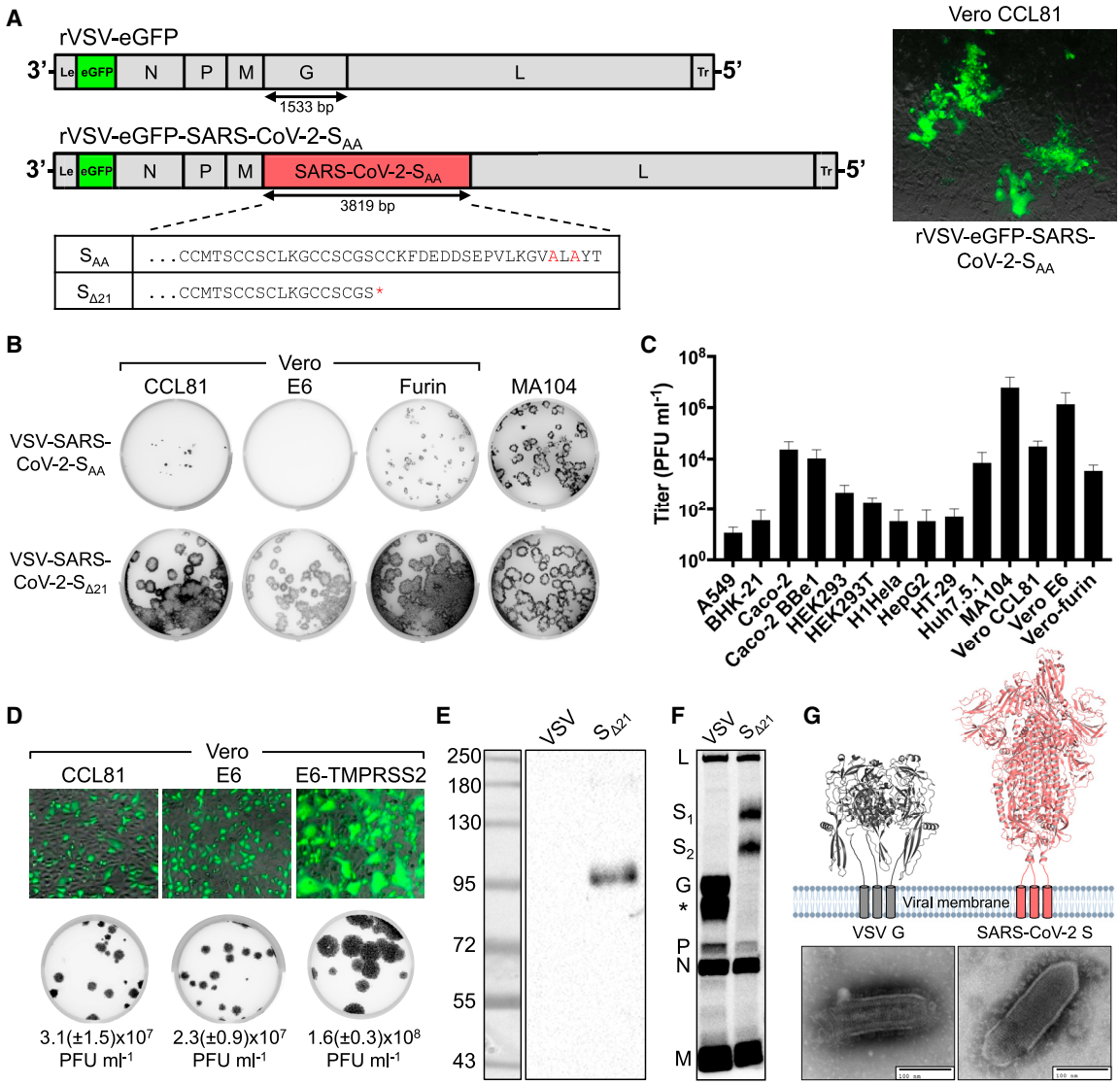

Figure 1. Generation and Characterization of an Infectious VSV-SARS-CoV-2 Chimera

(A) A schematic diagram depicting the genomic organization of the VSV recombinants. Shown 3′ to 5′ are the leader region (Le), eGFP, nucleocapsid (N), phosphoprotein (P), matrix (M), glycoprotein (G) or SARS-CoV-2 S, large polymerase (L), and trailer region (Tr). On right, infection of Vero CCL81 cells with supernatant from cells transfected with the eGFP reporter VSV-SARS-CoV-2-S_{AA}. Images were acquired 44 h post-infection (hpi) using a fluorescence microscope, and GFP and transmitted light images were merged using ImageJ. Shown at bottom, the alignment of the cytoplasmic tail of the VSV-SARS-CoV-2-S_{AA} and the sequence resulting from forward genetic selection of a mutant, which truncated the cytoplasmic tail by 21 amino acids. Mutations deviating from the wild-type spike are indicated in red, and an asterisk signifies a mutation to a stop codon.

(B) Plaque assays were performed to compare the spread of VSV-SARS-CoV-2-S_{AA} rescue supernatant and VSV-SARS-CoV-2-$S_{\Delta 21}$ on Vero CCL81, Vero E6, Vero-furin, and MA104 cells. Plates were scanned on a biomolecular imager and expression of eGFP is shown 92 hpi (representative images are shown; n > 3 except for S_{AA} on Vero E6, Vero-furin, and MA104 cells).

(C) The indicated cell types were infected with VSV-SARS-CoV-2-$S_{\Delta 21}$ at an MOI of 0.5. Cells and supernatants were harvested at 24 hpi and titrated on MA104 cells (data are pooled from three or more independent experiments; error bars indicate standard deviation of the mean.

(D Top: the indicated cells were infected with VSV-SARS-CoV-2-$S_{\Delta 21}$ at an MOI of 2. Images were acquired 7.5 hpi using a fluorescence microscope and GFP, and transmitted light images were processed and merged using ImageJ (data are representative of two independent experiments). Bottom: Plaque assays were performed on the indicated cell types using VSV-SARS-CoV-2-$S_{\Delta 21}$. Images showing GFP expression were acquired 48 hpi using a biomolecular imager (data are representative of at least three independent experiments; standard deviations of the mean are shown).

(E) Western blotting was performed on concentrated VSV-SARS-CoV-2-$S_{\Delta 21}$ and wild-type VSV particles on an 8% non-reducing SDS-PAGE gel. S1 was detected using a cross-reactive anti-SARS-CoV mAb (CR3022) (data are representative of two independent experiments).

(F) BSRT7/5 cells were inoculated at an MOI of 10 with VSV-eGFP, G-complemented VSV-SARS-CoV-2-$S_{\Delta 21}$, or mock infected (not shown), and were metabolically labeled with [^{35}S] methionine and cysteine for 20 h starting at 5 hpi in the presence of actinomycin D. Viral supernatants were analyzed by SDS-PAGE. A representative phosphor-image is shown from two independent experiments. An asterisk indicates a band that also was detected in the mock lane (not shown).

(G) Purified VSV-WT and VSV-SARS-CoV-2-$S_{\Delta 21}$ particles were subjected to negative stain electron microscopy; scale bars are equivalent to 100 nm. Prefusion structures of each respective glycoprotein are modeled above each EM image (PDB: 5I2S and 6VSB). See also Figures S1 and S2.

methionine metabolic labeling in BSRT7 cells, which support robust VSV replication, and analyzed released particles by SDS-PAGE and phosphorimaging. In addition to the VSV structural proteins (N, P, M, and L), two additional bands that correspond in size to glycosylated S1 (107 kDa) and $S2_{\Delta 21}$ (85 kDa) were observed for VSV-SARS-CoV-2-$S_{\Delta 21}$ (Figure 1F). Negative-stain electron microscopy of sucrose-gradient purified virus particles revealed that the membrane protein projecting from VSV-SARS-CoV-2-$S_{\Delta 21}$ is larger than observed on wild-type VSV particles (Figure 1G), which reflects the larger size of the coronavirus spike.

A High-Throughput Focus-Forming Assay with a Clinical Isolate of SARS-CoV-2

VSV-SARS-CoV-2-$S_{\Delta 21}$ has several advantages for detection and measuring of neutralizing antibodies, including lower biosafety containment level, ease of production and use, and rapid reporter gene readout. Nonetheless, the difference in virus morphology (spherical CoV versus bullet-shaped VSV) and possible effects on the conformational display of S on the virion surface raise questions of whether the accessibility of epitopes and stoichiometry of antibody neutralization is similar to authentic SARS-CoV-2. A direct comparison with a clinical isolate of SARS-CoV-2 is necessary to establish the utility of VSV-SARS-CoV-2-$S_{\Delta 21}$ for assays of viral entry and antibody neutralization.

We designed a high-throughput assay for titrating SARS-CoV-2 that could be applied to multiple cell substrates. Instead of using a plaque assay—which relies on the capacity for a virus to cause cell death, which can vary across cell types—we developed a focus-forming assay (FFA) and viral antigen detection as a measure of infectivity. We propagated SARS-CoV-2 in four different producer cell types (Vero CCL81, Vero E6, Vero-furin, and MA104 cells) and then measured the number and size of foci after staining recipient cells with an anti-S mAb. With SARS-CoV-2 stocks generated from each producer cell type, we observed distinct foci across recipient cell substrates at approximately 30 h post-inoculation (Figure 2A). We consistently observed the highest viral titers and largest foci sizes with Vero-furin and MA104 cells (Figures 2B and 2C). However, the larger foci were more difficult to enumerate on an automated Immunospot reader and required additional manual quality control analysis. Because of this, we used Vero E6 cells for our rapid focus-reduction neutralization tests (FRNT) in subsequent experiments.

A High-Throughput, eGFP-Based Neutralization Assay for VSV-SARS-CoV-2-$S_{\Delta 21}$

In parallel, we developed a high-throughput method to measure neutralization of VSV-SARS-CoV-2-$S_{\Delta 21}$. As VSV-SARS-CoV-2-$S_{\Delta 21}$ encodes an eGFP reporter and viral gene expression is robust, eGFP-positive cells can be quantified 7.5 h post-infection using a fluorescence microscope with automated counting analysis software. This approach enabled the development of an eGFP-reduction neutralization test (GRNT) (Figure 2D).

Neutralization of VSV-SARS-CoV-2-$S_{\Delta 21}$ and SARS-CoV-2 by Human Antibodies

Members of our group recently identified human mAbs from memory B cells of a SARS-CoV survivor that bind to SARS-CoV-2 S (Pinto et al., 2020). We tested a subset of these (mAbs 304, 306, 309, and 315) for their ability to inhibit VSV-SARS-CoV-2-$S_{\Delta 21}$ and SARS-CoV-2 infections on Vero E6 cells. While three of these mAbs showed poor inhibitory activity, mAb 309 potently neutralized both SARS-CoV-2 and VSV-SARS-CoV-2-$S_{\Delta 21}$ (Figures 3A and 3B) with similar EC_{50} values between the two assays (81 and 67 ng/mL for SARS-CoV-2 and VSV-SARS-CoV-2-$S_{\Delta 21}$, respectively). To broaden the test panel, we evaluated the activity of a panel of mAbs generated as part of a phage display library (Miersch et al., 2020) by both FRNT and GRNT. Many of these mAbs exhibited moderate neutralization activities in the EC_{50} range of 100 to 500 ng/mL (Figures 3C and 3D). Nonetheless, we observed the same neutralization trend between VSV-SARS-CoV-2-$S_{\Delta 21}$ and SARS-CoV-2 with highly correlated EC_{50} values (<2-fold differences).

Neutralization by Human ACE2-Fc Receptor Decoy Proteins

Human ACE2 (hACE2) is an entry receptor for both SARS-CoV and SARS-CoV-2 (Letko et al., 2020; Li et al., 2003, 2005; Wrapp et al., 2020). As a soluble hACE2-Fc decoy protein has been proposed as a therapeutic for SARS-CoV-2 (Kruse, 2020), in part based on its ability to inhibit SARS-CoV infection in cell culture (Moore et al., 2004), we tested whether hACE2-Fc could inhibit infection of VSV-SARS-CoV-2-$S_{\Delta 21}$ and SARS-CoV-2 using our FRNT and GRNT assays. When pre-mixed with VSV-SARS-CoV-2-$S_{\Delta 21}$ or SARS-CoV-2, hACE2-Fc, but not murine ACE2-Fc (mACE2-Fc), it dose dependently and equivalently inhibited infection of recipient Vero E6 cells (Figures 3E and 3F). As expected, hACE2-Fc did not inhibit infection of wild-type VSV, confirming that neutralization was specific to the SARS-CoV-2 S protein (Figure S3). We noted that a relatively high concentration of hACE2-Fc was required for inhibition, with EC_{50} values of 29 and 12.6 μg/mL for VSV-SARS-CoV-2-$S_{\Delta 21}$ and SARS-CoV-2, respectively. Thus, although soluble hACE2-Fc decoy proteins similarly inhibit infection of VSV-SARS-CoV-2-$S_{\Delta 21}$ and SARS-CoV-2, the potency is less than anticipated, which suggests that the receptor-binding domain (RBD) on the S protein on the surface of both viruses may not be fully accessible in solution.

Neutralization of VSV-SARS-CoV-2-$S_{\Delta 21}$ and SARS-CoV-2 by Human Immune Serum

As part of studies to evaluate immune convalescent plasma as a possible therapy for SARS-CoV-2-infected patients (Bloch et al., 2020), we obtained 42 serum samples from 20 individuals at different time points after the onset of COVID-19 symptoms (Table 1). These samples were pre-screened using a commercially available IgG ELISA. We tested each sample for neutralization of VSV-SARS-CoV-2-$S_{\Delta 21}$ and SARS-CoV-2 on Vero E6 cells. We observed that sera with ELISA-negative or indeterminate results generally showed low inhibitory titers (EC_{50} < 1/100), whereas ELISA-positive sera generated a broad range of neutralizing antibody activity (EC_{50} > 1/200 to > 1/1,900) (Figures 4A and S4). Remarkably, neutralization of VSV-SARS-CoV-2-$S_{\Delta 21}$ and SARS-CoV-2 was similar across the entire panel of samples (Figures 4B, 4C, and S4).

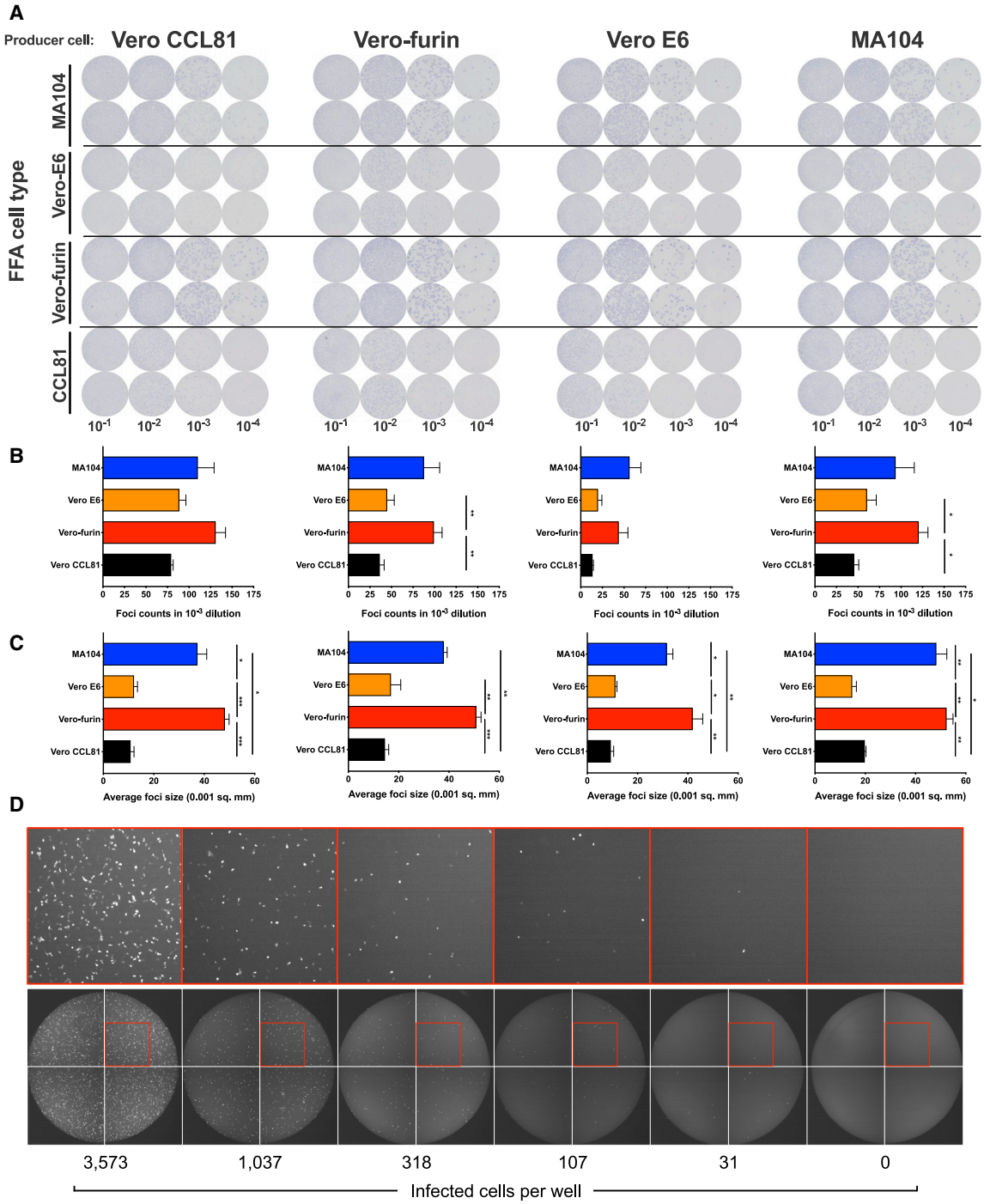

Figure 2. Development of a SARS-CoV-2 Focus-Forming Assay and a VSV-SARS-CoV-2-S$_{\Delta 21}$ eGFP-Reduction Assay

(A–C) Representative focus forming assay images (A) of viral stocks generated from each producer cell type (top) were developed on the indicated cell substrates (indicated on the left side). Data are representative of two independent experiments. Foci obtained in (A) were counted (B) and the size was determined (C) using an ImmunoSpot plate reader (*p < 0.05, **p < 0.01, ***p < 0.001 by one-way ANOVA with Tukey's multiple comparisons test; error bars indicate standard error of the mean).

(D) Representative serial dilution series of VSV-SARS-CoV-2-S$_{\Delta 21}$ on Vero E6 cells. The total number of infected cells per well was quantified using an automated microscope. Insets of enhanced magnification are shown in red. Data are representative of two independent experiments.

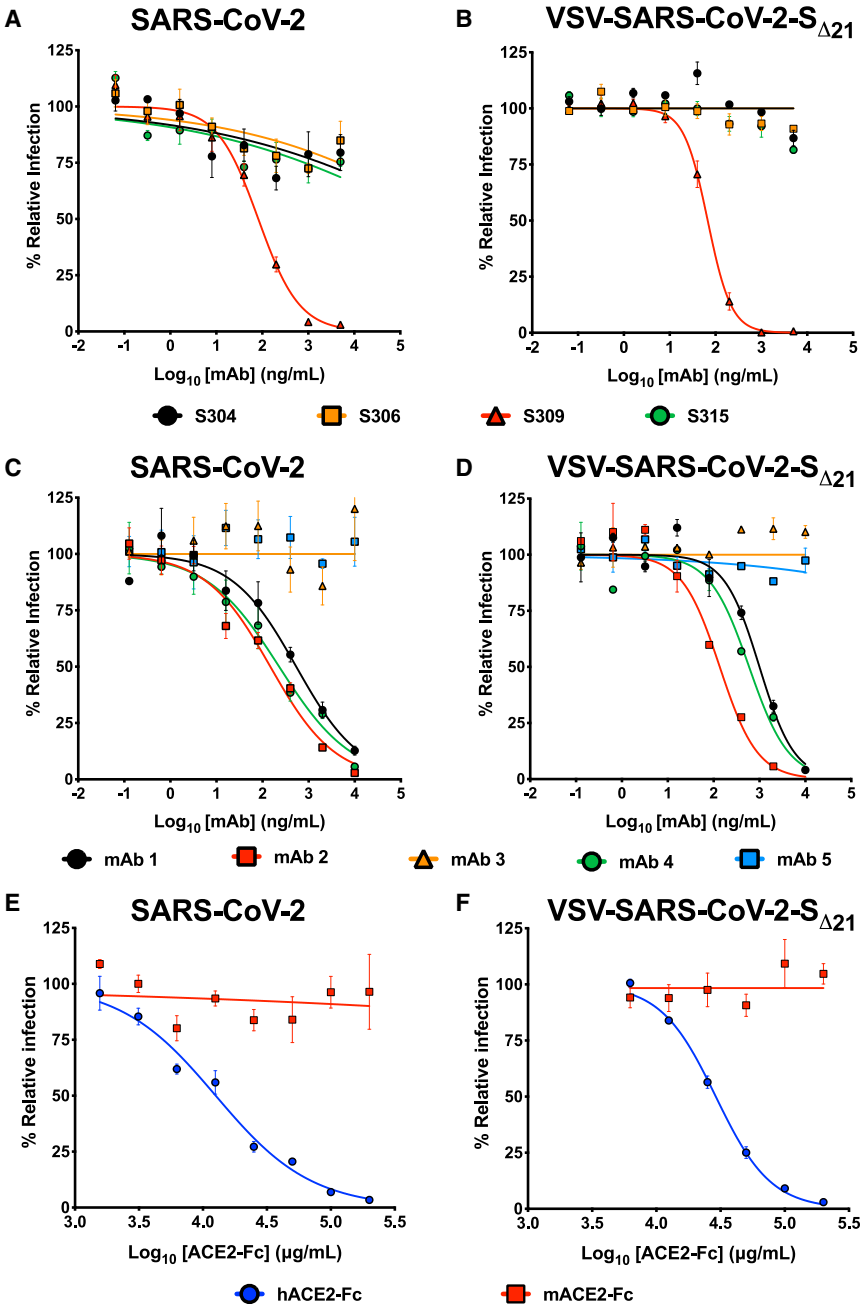

Figure 3. Neutralization of VSV-SARS-CoV-2-$S_{\Delta 21}$ and SARS-CoV-2 by Human Monoclonal Antibodies and hACE2 Decoy Receptors

(A and B) Cross-reactive mAbs isolated from a SARS-CoV survivor were tested for neutralizing activity against SARS-CoV-2 (A) or VSV-SARS-CoV-2-$S_{\Delta 21}$ (B) (n = 2 and 3, respectively).

(C and D) SARS-CoV-2 RBD-specific antibodies obtained from a phage library were tested for their capacity to neutralize SARS-CoV-2 (C) or VSV-SARS-CoV-2-$S_{\Delta 21}$ (D) (n = 2 and 2, respectively).

(E and F) hACE2-Fc or mACE2-Fc were tested for their neutralization activity against SARS-CoV-2 (E) or VSV-SARS-CoV-2-$S_{\Delta 21}$ (F) (n = 2 and 3, respectively).

Error bars in (A)–(F) represent the standard error of the mean. See also Figure S3.

SARS-CoV-2 infection in entry inhibition and neutralization studies.

DISCUSSION

Emerging viral pathogens have caused numerous epidemics and several pandemics over the last century. The most recent example, SARS-CoV-2, has spread to nearly every country in the world in just a few months, causing millions of infections and hundreds of thousands of deaths (https://www.worldometers.info/coronavirus/). Rapid responses to viral outbreaks and generation of countermeasures require readily accessible tools to facilitate study and evaluate antiviral activity. Here, we generated a high-titer, replication-competent chimeric VSV expressing the SARS-CoV-2 S protein that performs similarly to a SARS-CoV-2 clinical isolate across multiple neutralization tests. As access to BSL3 facilities is limited, the finding that VSV-SARS-CoV-2-$S_{\Delta 21}$ is neutralized similarly by decoy receptors, mAbs, and polyclonal antibodies in comparison to authentic SARS-CoV-2 is important. This tool will enable academic, government, and industry investigators to rapidly perform assays that interrogate SARS-CoV-2 entry, neutralization, and inhibition at a BSL2 level, which should simplify and expedite the discovery of therapeutic interventions and analysis of functional humoral immune responses.

VSV-SARS-CoV-2-$S_{\Delta 21}$ and SARS-CoV-2 Neutralization Assays Are Highly Correlative

We determined the extent to which the VSV-SARS-CoV-2-$S_{\Delta 21}$ and SARS-CoV-2 neutralization tests correlated with each other. We compared the GRNT and FRNT EC_{50} values obtained in assays with mAbs, polyclonal sera, and soluble ACE2 protein (Figure 5). For the samples with neutralizing activity, we observed a remarkably strong correlation between the two assays (r = 0.9285; $p < 0.001$). Moreover, all 11 of the samples that were deemed non-neutralizing in one assay had the same result in the second assay. Together, these results establish the utility of using VSV-SARS-CoV-2-$S_{\Delta 21}$ as a surrogate for authentic

Upon recovery of VSV-SARS-CoV-2-S_{AA}, we selected for a mutant, which contained a 21-amino acid deletion in the cytoplasmic tail. As truncation of the cytoplasmic tail eliminates the modified KxHxx ER retention signal, we suggest that this mutation facilitates more efficient incorporation of the SARS-CoV-2 S protein into the VSV particles. Although truncation of the cytoplasmic tail of HIV envelope protein resulted in conformational

Table 1. Human Serum ELISA IgG

Serum	Days Post Symptom Onset	Euroimmun IgG		Epitope IgG	
		Index	Reactive	Index	Reactive
1	14	1.3	+	2.6	+
2	12	6.0	+	3.5	+
3	17	10.2	+	3.9	+
4	16	14.9	+	4.5	+
5	5	0.2	–	1.2	+
6	19	8.6	+	4.4	+
7	17	7.1	+	4.1	+
8	10	5.1	+	2.0	+
9	14	6.8	+	3.1	+
10	6	0.2	–	1.1	+
11	-	5.6	+	0.9	+/–
12	-	<0.8	–	1.3	+
13	9	0.7	–	1.1	+
14	20	3.6	+	2.9	+
15	13	0.4	–	2.0	+
16	13	0.5	–	0.9	–
17	11	0.3	–	0.8	–
18	10	0.2	–	0.7	–
19	14	0.9	+/–	1.2	+
20	10	0.4	–	1.5	+
21	11	0.5	–	2.0	+
22	10	0.3	–	0.6	–
23	17	7.6	+	4.2	+
24	14	3.5	+	3.3	+
25	13	1.5	+	2.9	+
26	17	14.2	+	4.4	+
27	13	0.5	–	1.9	+
28	14	9.2	+	4.6	+
29	13	3.9	+	2.8	+
30	16	3.4	+	4.6	+
31	15	10.7	+	3.6	+
32	6	0.5	–	1.1	+
33	11	0.4	–	1.8	+
34	12	0.6	–	2.5	+
35	14	3.7	+	4.1	+
36	20	11.6	+	4.2	+
37	7	0.7	–	1.2	+
38	8	1.7	+	1.9	+
39	7	0.3	–	0.7	–
40	9	3.4	+	2.2	+
41	18	10.3	+	4.1	+
42	17	10.3	+	4.6	+

Serum samples from 20 individuals were collected at different time points post onset of COVID-19 symptoms and screened using two ELISA assays (Euroimmun or Epitope). The serum numbers correspond to those of Figures 4 and S3. IgG index values were calculated by dividing the O.D. of the serum sample by a reference O.D. control, and ratios were interpreted using the following criteria as recommended by the manufacturer: Negative (–) < 0.8, Indeterminate (+/–) 0.8–1.1, Positive (+) ≥ 1.1.

alterations in the ectodomain of the protein (Chen et al., 2015), based on the extensive neutralization data presented here, including correlation to neutralization of a clinical isolate of SARS CoV-2, a 21-amino acid truncation does not appear to substantively alter the structure of the S protein ectodomain. It remains to be determined whether fully wild-type S protein can incorporate efficiently into VSV. Indeed, similar mutations were generated in the SARS-CoV S protein cytoplasmic tail to boost incorporation into retroviruses and VSV pseudotypes (Fukushi et al., 2005; Giroglou et al., 2004; Moore et al., 2004).

The value of a chimeric virus depends on its capacity to present viral surface antigens in a similar way to its authentic counterpart (Garbutt et al., 2004). Indeed, the morphology of the bullet-shaped rhabdovirus and the spherical coronavirus and the density and geometry of S protein display could differentially impact antibody engagement and neutralization. Despite this concern, our extensive testing of VSV-SARS-CoV-2-$S_{\Delta 21}$ with antibodies and soluble ACE2-Fc proteins showed similar neutralization profiles compared to authentic, fully infectious SARS-CoV-2. Thus, VSV-SARS-CoV-2-$S_{\Delta 21}$, despite the structural differences of the virion, provides a useful tool for screening antibodies, entry-based antiviral agents, and vaccine responses against SARS-CoV-2. Indeed, convalescent plasma is under investigation as a potential COVID-19 therapeutic (Chen et al., 2020). Our studies suggest that, in addition to testing for anti-S or anti-RBD antibodies (Shen et al., 2020), neutralization assays with VSV-SARS-CoV-2-$S_{\Delta 21}$ may be a convenient and rapid method to obtain functional information about immune plasma preparations to enable prioritization prior to passive transfer to COVID-19 patients.

Coronaviruses possess a roughly 30 kb RNA genome, which requires that they encode a proofreading enzyme (ExoN in nsp14) (Denison et al., 2011) to counteract the error rate of the viral-RNA-dependent RNA polymerase. The lack of such proofreading enzymes in the genomes of rhabdoviruses suggests that selection of escape mutants to inhibitors of the coronavirus S protein will be faster in VSV-SARS-CoV-2, which further increases the utility of this chimeric virus. Our FRNT and GRNT assays can be used to establish evidence of prior SARS-CoV-2 infection or vaccination, as well as determine waning of functional responses over time, as the likelihood of cross-neutralizing responses with other cosmopolitan coronaviruses (*e.g.*, HCoV-229E and HCoV-OC43) is exceedingly low. Overall, VSV-SARS-CoV-2-$S_{\Delta 21}$ and our FRNT and GRNT assays can facilitate the development and evaluation of antibody- or entry-based countermeasures against SARS-CoV-2 infection. A similar VSV-SARS-CoV-2 chimera as a reporter of antibody mediated neutralization is described in a companion paper (Dieterle et al., 2020).

Limitations of Study

Our experiments do not directly test the safety of the recombinant VSV-eGFP-SARS-CoV-2. VSV-Indiana and chimeric VSV in which the native envelope protein is replaced with that of the envelope proteins of Ebola (Garbutt et al., 2004; Jones et al., 2005; Takada et al., 2003), Lassa (Geisbert et al., 2005), Andes (Brown et al., 2011), highly pathogenic avian influenza (Furuyama et al., 2020), and many other viruses are handled at BSL2. VSV-Ebola is a licensed human vaccine, ERVEBO, distributed by Merck. We

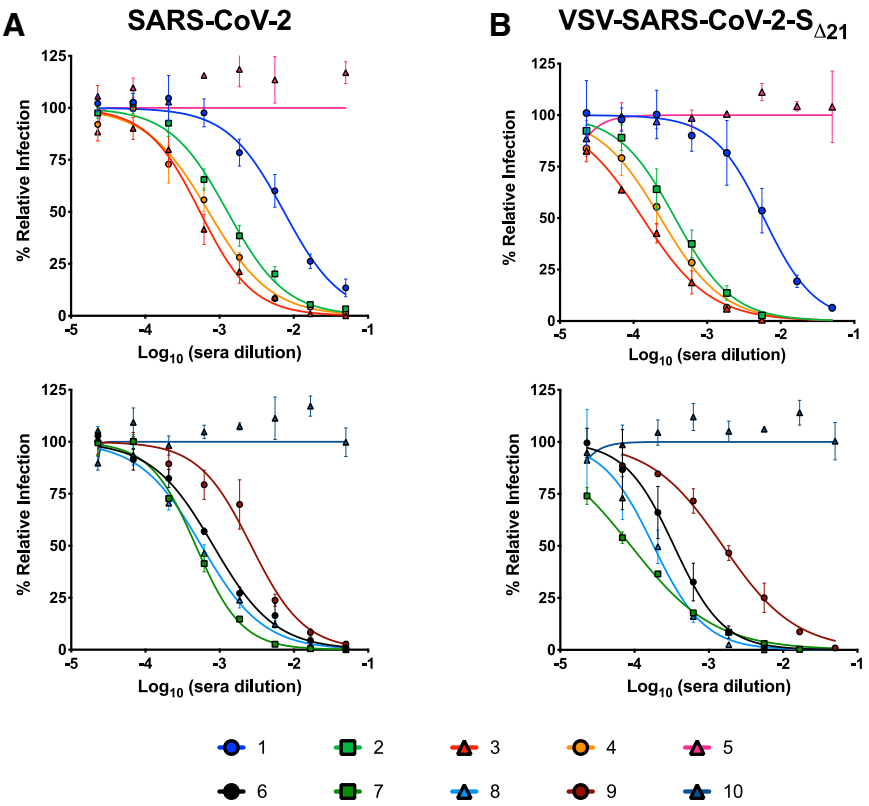

Figure 4. Human Immune Serum Neutralization of SARS-CoV-2 and VSV-SARS-CoV-2-S$_{\Delta21}$

(A and B) Representative neutralization curves of serum from SARS-CoV-2-infected donors with low, medium, and high inhibitory activity against SARS-CoV-2 (A) or VSV-SARS-CoV-2-S$_{\Delta21}$ (B) (n = 2 and 2, respectively). Error bars in (A) and (B) represent the standard error of the mean.

(C) EC$_{50}$ values of all human serum tested for neutralization of SARS-CoV-2 and VSV-SARS-CoV-2-S$_{\Delta21}$. Differences in the geometric mean or median titers were 3.0-fold between FRNT and GRNT assays. See also Figure S4.

are actively evaluating VSV-SARS-CoV-2 as a vaccine candidate, and mice inoculated with this virus do not develop disease (J.B.C., P.W.R., S.P.J.W., and M.S.D., unpublished data). Notwithstanding these data, a chimeric VSV containing both the F and G genes of Nipah virus remains pathogenic in mice (van den Pol et al., 2017), suggesting that appropriate caution should be used in handling VSV-SARS-CoV-2 at BSL2.

STAR★METHODS

Detailed methods are provided in the online version of this paper and include the following:

- KEY RESOURCES TABLE
- RESOURCE AVAILABILITY
  - Lead Contact
  - Materials Availability
  - Data and Code Availability
- EXPERIMENTAL MODEL AND SUBJECT DETAILS
  - Cells
  - Recombinant VSV
  - SARS-CoV-2
- METHOD DETAILS
  - Plasmids
  - Next Generation Sequencing
  - Western Blotting
  - Metabolic Radiolabeling of Virions
  - Transmission Electron Microscopy
  - Monoclonal Antibodies
  - Human Sera
  - Protein Expression and Purification
  - GFP-Reduction Neutralization Test
  - Focus-Reduction Neutralization Test
- QUANTIFICATION AND STATISTICAL ANALYSIS

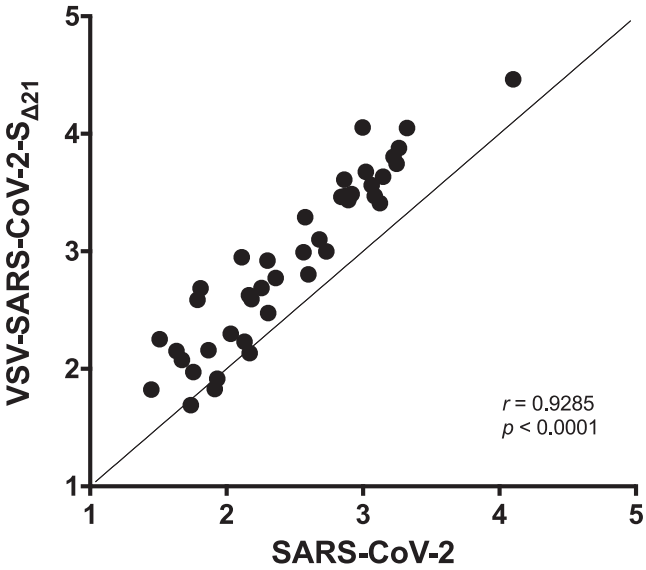

Figure 5. Correlation Analysis of Neutralization of SARS-CoV-2 and VSV-SARS-CoV-2-S$_{\Delta 21}$

EC_{50} values determined in Figures 3A–3D and 4A–4B were used to determine correlation between neutralization assays. Spearman's correlation *r* and *p* values are indicated.

SUPPLEMENTAL INFORMATION

Supplemental Information can be found online at https://doi.org/10.1016/j.chom.2020.06.021.

ACKNOWLEDGMENTS

This study was supported by NIH contracts and grants (75N93019C00062, HHSN272201700060C, R01 AI127828, R37 AI059371, and U01 AI151810), the Defense Advanced Research Project Agency (HR001117S0019), and gifts from Washington University in Saint Louis. J.B.C. is supported by a Helen Hay Whitney Foundation postdoctoral fellowship. We thank Natalie Thornburg for providing the clinical isolate of SARS-CoV-2, James Rini for providing RBD used to detect phage display mAbs, Jan Carette for providing A549 and H1Hela cells, Harry Greenberg for providing Huh7.5.1 and MA104 cells, and Stanley Perlman for providing Calu-3 cells. We also thank Wandy Beatty and the Molecular Microbiology Imaging Facility at the Washington University School of Medicine for taking the electron microscopy pictures. Some of the figures were created using BioRender.com.

AUTHOR CONTRIBUTIONS

J.B.C. performed SARS-CoV-2 neutralization experiments. P.W.R. generated and characterized VSV-SARS-CoV-2-S$_{\Delta 21}$ and performed neutralization experiments. R.E.C., Z.L., L.M.B., M.A.T., S.D., and Q.Z. provided experimental assistance. S.T., L.D., and D.W. prepared RNA-seq libraries and assembled the VSV-SARS-CoV-2-S$_{\Delta 21}$ sequence. H.Z. and D.H.F. generated and provided purified proteins; D.C. and H.W.V. provided the recombinant mAbs; S.M., M.U., S.S., and G.A. provided other recombinant mAbs; and E.S.T. and J.P.H. identified and provided the human immune serum. M.X.G.I. helped with automated microscope use and analysis. J.B.C., P.W.R., S.P.J.W., and M.S.D. wrote the initial draft, with the other authors providing editing comments.

DECLARATION OF INTERESTS

M.S.D. is a consultant for Inbios, Eli Lilly, Vir Biotechnology, and NGM Biopharmaceuticals and is on the Scientific Advisory Board of Moderna. The Diamond laboratory has received unrelated funding under sponsored research agreements from Moderna and Emergent BioSolutions. D.C. and H.W.V. are employees of Vir Biotechnology Inc. and may hold shares in Vir Biotechnology Inc. S.P.J.W. and P.W.R. have filed a disclosure with Washington University for the recombinant VSV.

Received: May 17, 2020
Revised: June 18, 2020
Accepted: June 24, 2020
Published: July 3, 2020

REFERENCES

Bai, Y., Yao, L., Wei, T., Tian, F., Jin, D.Y., Chen, L., and Wang, M. (2020). Presumed Asymptomatic Carrier Transmission of COVID-19. JAMA. https://doi.org/10.1001/jama.2020.2565.

Bankevich, A., Nurk, S., Antipov, D., Gurevich, A.A., Dvorkin, M., Kulikov, A.S., Lesin, V.M., Nikolenko, S.I., Pham, S., Prjibelski, A.D., et al. (2012). SPAdes: a new genome assembly algorithm and its applications to single-cell sequencing. J Comp. Biol. *19*, 455–477.

Bloch, E.M., Shoham, S., Casadevall, A., Sachais, B.S., Shaz, B., Winters, J.L., van Buskirk, C., Grossman, B.J., Joyner, M., Henderson, J.P., et al. (2020). Deployment of convalescent plasma for the prevention and treatment of COVID-19. J Clin Invest. *130*, 2757–2765.

Brown, K.S., Safronetz, D., Marzi, A., Ebihara, H., and Feldmann, H. (2011). Vesicular stomatitis virus-based vaccine protects hamsters against lethal challenge with Andes virus. J. Virol. *85*, 12781–12791.

Buchholz, U.J., Finke, S., and Conzelmann, K.K. (1999). Generation of bovine respiratory syncytial virus (BRSV) from cDNA: BRSV NS2 is not essential for virus replication in tissue culture, and the human RSV leader region acts as a functional BRSV genome promoter. J. Virol. *73*, 251–259.

Bushnell, B., Rood, J., and Singer, E. (2017). BBMerge - Accurate paired shotgun read merging via overlap. PLoS ONE *12*, e0185056.

Carette, J.E., Raaben, M., Wong, A.C., Herbert, A.S., Obernosterer, G., Mulherkar, N., Kuehne, A.I., Kranzusch, P.J., Griffin, A.M., Ruthel, G., et al. (2011). Ebola virus entry requires the cholesterol transporter Niemann-Pick C1. Nature *477*, 340–343.

Chandran, K., Sullivan, N.J., Felbor, U., Whelan, S.P., and Cunningham, J.M. (2005). Endosomal proteolysis of the Ebola virus glycoprotein is necessary for infection. Science *308*, 1643–1645.

Chen, J., Kovacs, J.M., Peng, H., Rits-Volloch, S., Lu, J., Park, D., Zablowsky, E., Seaman, M.S., and Chen, B. (2015). HIV-1 ENVELOPE. Effect of the cytoplasmic domain on antigenic characteristics of HIV-1 envelope glycoprotein. Science *349*, 191–195.

Chen, S., Zhou, Y., Chen, Y., and Gu, J. (2018). fastp: an ultra-fast all-in-one FASTQ preprocessor. Bioinformatics *34*, i884–i890.

Chen, L., Xiong, J., Bao, L., and Shi, Y. (2020). Convalescent plasma as a potential therapy for COVID-19. Lancet Infect. Dis. *20*, 398–400.

Delcher, A.L., Phillippy, A., Carlton, J., and Salzberg, S.L. (2002). Fast algorithms for large-scale genome alignment and comparison. Nucleic Acids Res. *30*, 2478–2483.

Denison, M.R., Graham, R.L., Donaldson, E.F., Eckerle, L.D., and Baric, R.S. (2011). Coronaviruses: an RNA proofreading machine regulates replication fidelity and diversity. RNA Biol. *8*, 270–279.

Dieterle, M.E., Haslwanter, D., Bortz, R.H., Wirchnianski, A.S., Lasso, G., Vergnolle, O., Abbasi, S.A., Fels, J.M., Laudermilch, E., Florez, C., et al. (2020). A replication-competent vesicular stomatitis virus for studies of SARS-CoV-2 spike-mediated cell entry and its inhibitionCell. Host & Microbe *28*, https://doi.org/10.1016/j.chom.2020.06.020.

Fuerst, T.R., Niles, E.G., Studier, F.W., and Moss, B. (1986). Eukaryotic transient-expression system based on recombinant vaccinia virus that synthesizes bacteriophage T7 RNA polymerase. Proc. Natl. Acad. Sci. USA *83*, 8122–8126.

Fukushi, S., Mizutani, T., Saijo, M., Matsuyama, S., Miyajima, N., Taguchi, F., Itamura, S., Kurane, I., and Morikawa, S. (2005). Vesicular stomatitis virus

pseudotyped with severe acute respiratory syndrome coronavirus spike protein. J. Gen. Virol. *86*, 2269–2274.

Fukushi, S., Mizutani, T., Saijo, M., Kurane, I., Taguchi, F., Tashiro, M., and Morikawa, S. (2006). Evaluation of a novel vesicular stomatitis virus pseudotype-based assay for detection of neutralizing antibody responses to SARS-CoV. J. Med. Virol. *78*, 1509–1512.

Furuyama, W., Reynolds, P., Haddock, E., Meade-White, K., Quynh Le, M., Kawaoka, Y., Feldmann, H., and Marzi, A. (2020). A single dose of a vesicular stomatitis virus-based influenza vaccine confers rapid protection against H5 viruses from different clades. NPJ Vaccines *5*, 4.

Garbutt, M., Liebscher, R., Wahl-Jensen, V., Jones, S., Möller, P., Wagner, R., Volchkov, V., Klenk, H.D., Feldmann, H., and Ströher, U. (2004). Properties of replication-competent vesicular stomatitis virus vectors expressing glycoproteins of filoviruses and arenaviruses. J. Virol. *78*, 5458–5465.

Geisbert, T.W., Jones, S., Fritz, E.A., Shurtleff, A.C., Geisbert, J.B., Liebscher, R., Grolla, A., Ströher, U., Fernando, L., Daddario, K.M., et al. (2005). Development of a new vaccine for the prevention of Lassa fever. PLoS Med. *2*, e183.

Giroglou, T., Cinatl, J., Jr., Rabenau, H., Drosten, C., Schwalbe, H., Doerr, H.W., and von Laer, D. (2004). Retroviral vectors pseudotyped with severe acute respiratory syndrome coronavirus S protein. J. Virol. *78*, 9007–9015.

Guan, W.J., Ni, Z.Y., Hu, Y., Liang, W.H., Ou, C.Q., He, J.X., Liu, L., Shan, H., Lei, C.L., Hui, D.S.C., et al.; China Medical Treatment Expert Group for Covid-19 (2020). Clinical Characteristics of Coronavirus Disease 2019 in China. N. Engl. J. Med. *382*, 1708–1720.

Hoffmann, M., Kleine-Weber, H., Schroeder, S., Krüger, N., Herrler, T., Erichsen, S., Schiergens, T.S., Herrler, G., Wu, N.H., Nitsche, A., et al. (2020). SARS-CoV-2 Cell Entry Depends on ACE2 and TMPRSS2 and Is Blocked by a Clinically Proven Protease Inhibitor. Cell *181*, 271–280.e8.

Jae, L.T., Raaben, M., Herbert, A.S., Kuehne, A.I., Wirchnianski, A.S., Soh, T.K., Stubbs, S.H., Janssen, H., Damme, M., Saftig, P., et al. (2014). Virus entry. Lassa virus entry requires a trigger-induced receptor switch. Science *344*, 1506–1510.

Jones, S.M., Feldmann, H., Ströher, U., Geisbert, J.B., Fernando, L., Grolla, A., Klenk, H.D., Sullivan, N.J., Volchkov, V.E., Fritz, E.A., et al. (2005). Live attenuated recombinant vaccine protects nonhuman primates against Ebola and Marburg viruses. Nat. Med. *11*, 786–790.

Kobinger, G.P., Limberis, M.P., Somanathan, S., Schumer, G., Bell, P., and Wilson, J.M. (2007). Human immunodeficiency viral vector pseudotyped with the spike envelope of severe acute respiratory syndrome coronavirus transduces human airway epithelial cells and dendritic cells. Hum. Gene Ther. *18*, 413–422.

Kruse, R.L. (2020). Therapeutic strategies in an outbreak scenario to treat the novel coronavirus originating in Wuhan, China. F1000Res. *9*, 72.

Lei, C., Qian, K., Li, T., Zhang, S., Fu, W., Ding, M., and Hu, S. (2020). Neutralization of SARS-CoV-2 spike pseudotyped virus by recombinant ACE2-Ig. Nat. Commun. *11*, 2070.

Letko, M., Marzi, A., and Munster, V. (2020). Functional assessment of cell entry and receptor usage for SARS-CoV-2 and other lineage B betacoronaviruses. Nat. Microbiol. *5*, 562–569.

Li, W., Moore, M.J., Vasilieva, N., Sui, J., Wong, S.K., Berne, M.A., Somasundaran, M., Sullivan, J.L., Luzuriaga, K., Greenough, T.C., et al. (2003). Angiotensin-converting enzyme 2 is a functional receptor for the SARS coronavirus. Nature *426*, 450–454.

Li, F., Li, W., Farzan, M., and Harrison, S.C. (2005). Structure of SARS coronavirus spike receptor-binding domain complexed with receptor. Science *309*, 1864–1868.

Li, J., Wang, J.T., and Whelan, S.P. (2006). A unique strategy for mRNA cap methylation used by vesicular stomatitis virus. Proc. Natl. Acad. Sci. USA *103*, 8493–8498.

Li, H., Handsaker, B., Wysoker, A., Fennell, T., Ruan, J., Homer, N., Marth, G., Abecasis, G., and Durbin, R.; 1000 Genome Project Data Processing Subgroup (2009). The Sequence Alignment/Map format and SAMtools. Bioinformatics *25*, 2078–2079.

Lontok, E., Corse, E., and Machamer, C.E. (2004). Intracellular targeting signals contribute to localization of coronavirus spike proteins near the virus assembly site. J. Virol. *78*, 5913–5922.

McBride, C.E., Li, J., and Machamer, C.E. (2007). The cytoplasmic tail of the severe acute respiratory syndrome coronavirus spike protein contains a novel endoplasmic reticulum retrieval signal that binds COPI and promotes interaction with membrane protein. J. Virol. *81*, 2418–2428.

Miersch, S., Ustav, M.J., Li, Z., Case, J.B., Ganaie, S., Matusali, G., Colavita, F., Lapa, D., Capobianchi, M.R., Novelli, G., et al. (2020). Synthetic antibodies neutralize SARS-CoV-2 infection of mammalian cells. bioRxiv. https://doi.org/10.1101/2020.06.05.137349.

Moore, M.J., Dorfman, T., Li, W., Wong, S.K., Li, Y., Kuhn, J.H., Coderre, J., Vasilieva, N., Han, Z., Greenough, T.C., et al. (2004). Retroviruses pseudotyped with the severe acute respiratory syndrome coronavirus spike protein efficiently infect cells expressing angiotensin-converting enzyme 2. J. Virol. *78*, 10628–10635.

Mukherjee, S., Sirohi, D., Dowd, K.A., Chen, Z., Diamond, M.S., Kuhn, R.J., and Pierson, T.C. (2016). Enhancing dengue virus maturation using a stable furin over-expressing cell line. Virology *497*, 33–40.

Nie, J., Li, Q., Wu, J., Zhao, C., Hao, H., Liu, H., Zhang, L., Nie, L., Qin, H., Wang, M., et al. (2020). Establishment and validation of a pseudovirus neutralization assay for SARS-CoV-2. Emerg. Microbes Infect. *9*, 680–686.

Ou, X., Liu, Y., Lei, X., Li, P., Mi, D., Ren, L., Guo, L., Guo, R., Chen, T., Hu, J., et al. (2020). Characterization of spike glycoprotein of SARS-CoV-2 on virus entry and its immune cross-reactivity with SARS-CoV. Nat. Commun. *11*, 1620.

Persson, H., Ye, W., Wernimont, A., Adams, J.J., Koide, A., Koide, S., Lam, R., and Sidhu, S.S. (2013). CDR-H3 diversity is not required for antigen recognition by synthetic antibodies. J. Mol. Biol. *425*, 803–811.

Pinto, D., Park, Y.J., Beltramello, M., Walls, A.C., Tortorici, M.A., Bianchi, S., Jaconi, S., Culap, K., Zatta, F., De Marco, A., et al. (2020). Cross-neutralization of SARS-CoV-2 by a human monoclonal SARS-CoV antibody. Nature *583*, 290–295.

Raj, V.S., Mou, H., Smits, S.L., Dekkers, D.H., Müller, M.A., Dijkman, R., Muth, D., Demmers, J.A., Zaki, A., Fouchier, R.A., et al. (2013). Dipeptidyl peptidase 4 is a functional receptor for the emerging human coronavirus-EMC. Nature *495*, 251–254.

Ruch, T.R., and Machamer, C.E. (2012). The coronavirus E protein: assembly and beyond. Viruses *4*, 363–382.

Shen, C., Wang, Z., Zhao, F., Yang, Y., Li, J., Yuan, J., Wang, F., Li, D., Yang, M., Xing, L., et al. (2020). Treatment of 5 Critically Ill Patients With COVID-19 With Convalescent Plasma. JAMA *323*, 1582–1589.

Stanifer, M.L., Cureton, D.K., and Whelan, S.P. (2011). A recombinant vesicular stomatitis virus bearing a lethal mutation in the glycoprotein gene uncovers a second site suppressor that restores fusion. J. Virol. *85*, 8105–8115.

Stettler, K., Beltramello, M., Espinosa, D.A., Graham, V., Cassotta, A., Bianchi, S., Vanzetta, F., Minola, A., Jaconi, S., Mele, F., et al. (2016). Specificity, cross-reactivity, and function of antibodies elicited by Zika virus infection. Science *353*, 823–826.

Takada, A., Feldmann, H., Stroeher, U., Bray, M., Watanabe, S., Ito, H., McGregor, M., and Kawaoka, Y. (2003). Identification of protective epitopes on ebola virus glycoprotein at the single amino acid level by using recombinant vesicular stomatitis viruses. J. Virol. *77*, 1069–1074.

Tao, Y., Mis, M., Blazer, L., Ustav, M., Jnr, Steinhart, Z., Chidiac, R., Kubarakos, E., O'Brien, S., Wang, X., Jarvik, N., et al. (2019). Tailored tetravalent antibodies potently and specifically activate Wnt/Frizzled pathways in cells, organoids and mice. eLife *8*, e46134.

ter Meulen, J., van den Brink, E.N., Poon, L.L., Marissen, W.E., Leung, C.S., Cox, F., Cheung, C.Y., Bakker, A.Q., Bogaards, J.A., van Deventer, E., et al. (2006). Human monoclonal antibody combination against SARS coronavirus: synergy and coverage of escape mutants. PLoS Med. *3*, e237.

Tortorici, M.A., and Veesler, D. (2019). Structural insights into coronavirus entry. Adv. Virus Res. *105*, 93–116.

Traggiai, E., Becker, S., Subbarao, K., Kolesnikova, L., Uematsu, Y., Gismondo, M.R., Murphy, B.R., Rappuoli, R., and Lanzavecchia, A. (2004). An efficient method to make human monoclonal antibodies from memory B cells: potent neutralization of SARS coronavirus. Nat. Med. *10*, 871–875.

van den Pol, A.N., Mao, G., Chattopadhyay, A., Rose, J.K., and Davis, J.N. (2017). Chikungunya, Influenza, Nipah, and Semliki Forest Chimeric Viruses with Vesicular Stomatitis Virus: Actions in the Brain. J. Virol. *91*, e02154-16.

Walls, A.C., Park, Y.J., Tortorici, M.A., Wall, A., McGuire, A.T., and Veesler, D. (2020). Structure, Function, and Antigenicity of the SARS-CoV-2 Spike Glycoprotein. Cell *181*, 281–292.e6.

Watanabe, Y., Allen, J.D., Wrapp, D., McLellan, J.S., and Crispin, M. (2020). Site-specific glycan analysis of the SARS-CoV-2 spike. Science, eabb9983.

Whelan, S.P., Ball, L.A., Barr, J.N., and Wertz, G.T. (1995). Efficient recovery of infectious vesicular stomatitis virus entirely from cDNA clones. Proc. Natl. Acad. Sci. USA *92*, 8388–8392.

Wrapp, D., Wang, N., Corbett, K.S., Goldsmith, J.A., Hsieh, C.L., Abiona, O., Graham, B.S., and McLellan, J.S. (2020). Cryo-EM structure of the 2019-nCoV spike in the prefusion conformation. Science.

Yuan, M., Wu, N.C., Zhu, X., Lee, C.D., So, R.T.Y., Lv, H., Mok, C.K.P., and Wilson, I.A. (2020). A highly conserved cryptic epitope in the receptor binding domains of SARS-CoV-2 and SARS-CoV. Science *368*, 630–633.

Zang, R., Gomez Castro, M.F., McCune, B.T., Zeng, Q., Rothlauf, P.W., Sonnek, N.M., Liu, Z., Brulois, K.F., Wang, X., Greenberg, H.B., et al. (2020). TMPRSS2 and TMPRSS4 promote SARS-CoV-2 infection of human small intestinal enterocytes. Sci. Immunol. *5*, eabc3582.

Zhang, T., Wu, Q., and Zhang, Z. (2020). Probable Pangolin Origin of SARS-CoV-2 Associated with the COVID-19 Outbreak. Curr Biol. *30*, 1346–1351.e2.

Zhou, P., Yang, X.L., Wang, X.G., Hu, B., Zhang, L., Zhang, W., Si, H.R., Zhu, Y., Li, B., Huang, C.L., et al. (2020). A pneumonia outbreak associated with a new coronavirus of probable bat origin. Nature *579*, 270–273.

STAR★METHODS

KEY RESOURCES TABLE

REAGENT or RESOURCE	SOURCE	IDENTIFIER
Antibodies		
Anti-human IgG peroxidase	Sigma-Aldrich	Cat# A6029-1ML; RRID: AB_258272
CR3022	ter Meulen et al., 2006; Yuan et al., 2020	N/A
Goat anti-human IgG - H&L (HRP)	Abcam	Cat# ab6858-1MG; RRID: AB_955433
Phage display antibody set	Miersch et al., Bioraxiv https://doi.org/10.1101/2020.06.05.137349	N/A
VIR antibody set	Pinto et al., 2020	S309 PDB: 6WS6
Bacterial and Virus Strains		
2019 n-CoV/USA_WA1/2020	CDC (gift from Natalie Thornburg)	N/A
Vaccinia virus vTF7-3	Fuerst et al., 1986	N/A
VSV-eGFP	Chandran et al., 2005	N/A
Biological Samples		
Patient serum set	This study	N/A
Chemicals, Peptides, and Recombinant Proteins		
Blasticidin S HCl	GIBCO/Thermo Fisher	Cat# A1113903
Cytosine arabinoside	Sigma-Aldrich	Cat# C1768
Formaldehyde Solution	Millipore Sigma	Cat# FX0410-5
HEPES, free acid	Millipore Sigma	Cat #5310-OP
Hoechst 33342	Invitrogen/Thermo Fisher	Cat# H3570
Human ACE2-Fc	This study	GenBank: BAB40370.1 & AAC82527.1
L-[^{35}S]-cysteine	Perkin Elmer	Cat# NEG022T
L-[^{35}S]-methionine	Perkin Elmer	Cat# NEG009T
Lipofectamine 2000 Transfection Reagent	Invitrogen/Thermo Fisher	Cat# 11668019
Mouse ACE2-Fc	This study	NCBI Reference Sequence: NP_001123985.1
Phosphotungstic acid hydrate	Sigma-Aldrich	Cat# 79690-25G
Pierce ECL Western Blotting Substrate	Thermo Scientific/Thermo Fisher	Cat# 32106
Protein A Agarose Resin	GoldBio	Cat# P-400-100
TRIzol Reagent	Invitrogen/Thermo Fisher	Cat# 15596018
TrueBlue peroxidase substrate	KPL/SeraCare	Cat# 5510-0050
Critical Commercial Assays		
Anti-SARS-CoV-2 ELISA (IgG) serology test	Euroimmun US, Inc., 1 Bloomfield Ave, Mountain Lakes, NJ 07046	N/A
Deposited Data		
Nucleotide sequence of VSV-eGFP-SARS-CoV-2-S$_{\Delta 21}$	This study	BioProject: PRJNA635934; SRA: SRR11878607
Experimental Models: Cell Lines		
A549	Gift from Jan Carette	N/A
BHK-21	ATCC	Cat# CCL-10
BSRT7/5	Buchholz et al., 1999	N/A
Caco-2	ATCC	Cat# HTB-37
Caco-2 BBe1	ATCC	Cat# CRL-2102
Calu-3	Gift from Stanley Perlman	N/A
Expi293F	Thermo Fisher	Cat# A14527

(*Continued on next page*)

Continued

REAGENT or RESOURCE	SOURCE	IDENTIFIER
ExpiCHO	GIBCO/Thermo Fisher	Cat# A29127
HEK293	ATCC	Cat# CRL-1573
HEK293T	ATCC	Cat# CRL-3216
H1Hela	Gift from Jan Carette	N/A
HepG2	ATCC	Cat# HB-8065
HT-29	ATCC	Cat# HTB-38
Huh7.5.1	Gift from Harry Greenberg	
MA104	Gift from Harry Greenberg	N/A
Vero CCL81	ATCC	Cat# CCL-81
Vero E6	ATCC	Cat# CRL-1586
Vero E6-TMPRSS2	This paper	N/A
Vero-furin	Mukherjee et al., 2016	N/A
Experimental Models: Organisms/Strains		
N/A	N/A	N/A
Oligonucleotides		
TruSeq RNA Single Indexes Set A	Illumina	Cat# 20020492
TruSeq RNA Single Indexes Set B	Illumina	Cat# 20020493
Recombinant DNA		
pCAGGS-VSV-G	Stanifer et al., 2011	N/A
pFM1.2-hACE2-Fc	This paper	GenBank: AB046569.1
pFM1.2-mACE2-Fc	This paper	NCBI Reference Sequence: NM_001130513.1
pGEM3-VSV L	Whelan et al., 1995	N/A
pGEM3-VSV G	Stanifer et al., 2011	N/A
pGEM3-VSV N	Whelan et al., 1995	N/A
pGEM3-VSV P	Whelan et al., 1995	N/A
pLX304-TMPRSS2	Zang et al., 2020	N/A
psPAX2	Gift from Didier Trono (unpublished data)	Addgene Cat# 12260
pVSV-eGFP	Chandran et al., 2005	N/A
pVSV-eGFP-SARS-CoV-2-S_{AA}	This study	Spike mutated from MN908947.3
pVSV-eGFP-SARS-CoV-2-S MERS S_{AA} cytoplasmic tail switch	This paper	Spike mutated from a codon-optimized version of AHI48572.1
pVSV-eGFP-SARS-CoV-2-S VSV G #1 cytoplasmic tail switch	This paper	VSV Indiana G (strain Orsay)
pVSV-eGFP-SARS-CoV-2-S VSV G #2 cytoplasmic tail switch	This paper	VSV Indiana G (strain Orsay)
pVSV-eGFP-SARS-CoV-2-S VSV G Ecto/TM/tail switch	This paper	VSV Indiana G (strain Orsay)
pVSV-eGFP-SARS-CoV-2-S VSV G TM/tail switch	This paper	VSV Indiana G (strain Orsay)
Software and Algorithms		
BBMap 38.79	Bushnell et al., 2017	https://jgi.doe.gov/data-and-tools/bbtools/
Fastp 0.20.0	Chen et al., 2018	https://github.com/OpenGene/fastp
Image Analyses: GE InCell Analyzer 1000 Workstation	GE Life Sciences (now Cytiva)	N/A
NUCmer 3.1	Delcher et al., 2002	http://mummer.sourceforge.net/
SAMtools 1.9	Li et al., 2009	http://www.htslib.org/
SPAdes 3.13.0	Bankevich et al., 2012	http://cab.spbu.ru/software/spades/

(*Continued on next page*)

Continued

REAGENT or RESOURCE	SOURCE	IDENTIFIER
Statistics: Prism 8.0	GraphPad	N/A
Other		
TruSeq Stranded Total RNA Library Prep Kit with Ribo-Zero Human/Mouse/Rat	Illumina	Cat #20020596

RESOURCE AVAILABILITY

Lead Contact

Further information and requests for resources and reagents should be directed to and will be fulfilled by the Lead Contact author Sean P.J. Whelan (spjwhelan@wustl.edu).

Materials Availability

All plasmids, antibodies, cells, viruses, and cell lines developed are available under Material Transfer Agreements from Washington University School of Medicine.

Data and Code Availability

The authors declare that all data supporting the findings of this study are available within the paper. The sequence of VSV-eGFP-SARS-CoV-2-$S_{\Delta 21}$ (passage 12) generated during this study is available through NCBI (SRA: SRR11878607, https://www.ncbi.nlm.nih.gov/sra/?term=SRR11878607; BioProject: PRJNA635934).

EXPERIMENTAL MODEL AND SUBJECT DETAILS

Cells

Cells were maintained in humidified incubators at 34 or 37°C and 5% CO_2 in the indicated media. BSRT7/5, Vero CCL81, Vero E6, Vero E6-TMPRSS2, A549, Caco-2, Caco-2 BBe1, Calu-3, Huh7.5.1, HepG2, H1Hela, BHK-21, HEK293, and HEK293T were maintained in DMEM (Corning or VWR) supplemented with glucose, L-glutamine, sodium pyruvate, and 10% fetal bovine serum (FBS). Vero-furin cells (Mukherjee et al., 2016) also were supplemented with 5 μg/mL of Blasticidin S HCl (GIBCO). MA104 cells were maintained in Medium 199 (GIBCO) containing 10% FBS. HT-29 cells were cultured in complete DMEM/F12 (Thermo Fisher) supplemented with sodium pyruvate, non-essential amino acids, and HEPES (Millipore Sigma). Vero E6-TMPRSS2 cells were generated using a lentivirus vector. Briefly, HEK293T producer cells were transfected with pLX304-TMPRSS2, pCAGGS-VSV-G, and psPAX2, and cell culture supernatants were collected at 48 h and clarified by centrifugation at 1,000 x g for 5 min. The resulting lentivirus was used to infect Vero E6 cells for 24 h, and cells were selected with 40 μg/mL Blasticidin S HCl for 7 days.

Recombinant VSV

Recovery of recombinant VSV was performed as described (Whelan et al., 1995). Briefly, BSRT7/5 cells (Buchholz et al., 1999) were inoculated with vaccinia virus vTF7-3 (Fuerst et al., 1986) and subsequently transfected with T7-expression plasmids encoding VSV N, P, L, and G, and an antigenomic copy of the viral genome. Cell culture supernatants were collected at 56-72 h, clarified by centrifugation (5 min at 1,000 x g), and filtered through a 0.22 μm filter. Virus was plaque-purified on Vero CCL81 cells in the presence of 25 μg/mL of cytosine arabinoside (Sigma-Aldrich), and plaques in agarose plugs were amplified on Vero CCL81 cells. Viral stocks were amplified on MA104 cells at an MOI of 0.01 in Medium 199 containing 2% FBS and 20 mM HEPES pH 7.7 at 34°C. Viral supernatants were harvested upon extensive cytopathic effect and clarified of cell debris by centrifugation at 1,000 x g for 5 min. Aliquots were maintained at −80°C. Construction and use of VSV-SARS-CoV-2 was approved by the Washington University School of Medicine Institutional Biosafety Committee at Biosafety level 2.

SARS-CoV-2

SARS-CoV-2 strain 2019 n-CoV/USA_WA1/2020 was obtained from the Centers for Disease Control and Prevention (gift of Natalie Thornburg). Virus was passaged in the indicated producer cells (Figures 2A–2C). Work with SARS-CoV-2 was approved by the Washington University School of Medicine Institutional Biosafety Committee at Biosafety level 3 with positive pressure respirators.

METHOD DETAILS

Plasmids

The S gene of SARS-CoV-2 isolate Wuhan-Hu-1 (GenBank MN908947.3) was synthesized in two fragments (Integrated DNA Technologies) and inserted into an infectious molecular clone of VSV (Chandran et al., 2005; Whelan et al., 1995) as previously (Carette et al., 2011; Jae et al., 2014). Modifications to the cytoplasmic tail were assembled identically, and accession numbers or references

to the amino acid sequences used for the MERS and VSV G tail mutants can be found in the Key Resources Table. Other plasmids were previously described: VSV N, P, L and G expression plasmids (Stanifer et al., 2011; Whelan et al., 1995), psPAX2 (Addgene), and pLX304-TMPRSS2 (Zang et al., 2020).

Next Generation Sequencing

Total RNA was extracted from Vero CCL81 cells infected with VSV-SARS-CoV-2-$S_{\Delta 21}$ using TRIzol (Invitrogen) according to the manufacturer's protocol. RNA was used to generate next generation sequencing libraries using TruSeq Stranded Total RNA library kit with Ribo Zero ribosomal subtraction (Illumina). The libraries were quantified using a bioanalyzer (Agilent) and pooled at an equal molar concentration and used to generate paired end 250 bp reads on a MiSeq (Illumina). Raw sequencing data was processed using fastp v0.20.0 (Chen et al., 2018) to cut adaptor sequences and filter out sequences with a Phred quality score < 30. Processed reads were aligned to the reference plasmid sequence using BBMap v38.79 (Bushnell et al., 2017). Reads that mapped to the reference were extracted using SAMtools 1.9 (Li et al., 2009). The extracted mapped reads were used as input for *de novo* assembly with SPAdes v3.13.0 (Bankevich et al., 2012). Assembled contigs produced a 14.2 kb consensus sequence, which was subsequently aligned to the reference plasmid using NUCmer v3.1 (Delcher et al., 2002). Consensus sequences for each RNA sample were generated by aligning contigs to the reference plasmid sequence pVSV(1+)-eGFP-SARS-CoV-2-S with SnapGene v5.0.

Western Blotting

Purified VSV virions were incubated in non-reducing denaturation buffer (55 mM Tris-HCl pH 6.8, 1.67% (w/v) SDS, 7.5% (w/v) glycerol) at 100°C for 5 min. Viral proteins were separated on a 8% acrylamide gel, transferred onto a nitrocellulose membrane, and incubated with human anti-SARS antibody CR3022 diluted in Tris-buffered saline containing 1% Tween-20 (TBS-T) and 5% milk, followed by incubation with HRP-conjugated goat anti-human antibody (Abcam) diluted in TBS-T containing 1% milk. HRP activity was visualized using the Pierce ECL western blotting kit (Thermo Scientific) and imaged with a ChemiDocTM MP Imager (Bio-Rad).

Metabolic Radiolabeling of Virions

To generate high titer stocks of VSV-SARS-CoV-2, BSRT7/5 cells were transfected with pCAGGS-VSV-G in Opti-MEM (GIBCO) using Lipofectamine 2000 (Invitrogen) and infected 7 h later with VSV-SARS-CoV-2-$S_{\Delta 21}$ at an MOI of 0.1 in DMEM containing 2% FBS and 20 mM HEPES pH 7.7. Viral stocks were collected at 48 hpi, and used to infect fresh cells (MOI of 10) for labeling of viral proteins. At 4 hpi, cells were starved in serum free, methionine/cysteine free DMEM (Corning), and exposed to 15 μCi/mL [^{35}S]-methionine and [^{35}S]-cysteine (Perkin Elmer) from 5-24 h in the presence of actinomycin D. Cell culture supernatants were collected, clarified by centrifugation (1,500 x g, 5 min), and analyzed by SDS-PAGE and detected by phosphoimage analysis (Li et al., 2006).

Transmission Electron Microscopy

Purified viruses were adhered to glow-discharged, carbon-coated copper grids. Samples were stained with 2% (w/v) phosphotungstic acid (Sigma-Aldrich), pH 7.1, in H_2O and viewed on a JEOL 1200 EX transmission electron microscope (JEOL USA Inc.) equipped with an AMT 8-megapixel digital camera and AMT Image Capture Engine V602 software (Advanced Microscopy Techniques).

Monoclonal Antibodies

Phage-displayed Fab libraries were panned against immobilized SARS-CoV-2 spike RBD in multiple rounds using established methods (Persson et al., 2013). Following four rounds of selection, phage ELISAs were used to screen 384 clones to identify those that bound specifically to RBD. The complementarity determining regions of Fab-phage clones were decoded by sequencing the variable regions and cloning them into mammalian expression vectors for expression and purification of human IgG1 proteins, as described (Tao et al., 2019). A subset of the panel of mAbs was tested for neutralization as a part of this study.

Another set of mAbs (S304, S306, S309, S310 and S315) were isolated from EBV-immortalized memory B cells from a SARS-CoV survivor (Traggiai et al., 2004) and are cross-reactive to SARS-CoV-2 (Pinto et al., 2020). Recombinant antibodies were expressed in ExpiCHO cells transiently co-transfected with plasmids expressing the heavy and light chain as previously described (Stettler et al., 2016).

Human Sera

Human samples were collected from PCR-confirmed COVID-19 patients. Serum samples were obtained by routine phlebotomy at different days post symptom onset (range: day 5 - 20). Samples were prescreened by the Euroimmun anti-SARS-CoV-2 IgG ELISA (Lubeck, Germany), a qualitative assay with the Food and Drug Administration Emergency Use Authorization that detects antibodies to the SARS-CoV-2 S protein. This study was approved by the Mayo Clinic Institutional Review Board.

Protein Expression and Purification

DNA fragments encoding human ACE2 (hACE2 residues 1-615) and mouse ACE2 (mACE2, residues 1-615) were synthesized and cloned into pFM1.2 with a C-terminal HRV-3C protease cleavage site (LEVLFQGP) and a human IgG1 Fc region as previously described (Raj et al., 2013). We transiently transfected plasmids into Expi293F cells and harvested cell supernatants 4 days post transfection. Secreted hACE2-Fc and mACE2-Fc proteins were purified by protein A chromatography (GoldBio).

GFP-Reduction Neutralization Test

Patient samples were heat-inactivated at 56°C for 30 min. Indicated dilutions of samples were incubated with 10^2 PFU of VSV-SARS-CoV-2-$S_{\Delta 21}$ for 1 h at 37°C. Antibody-virus complexes were added to Vero E6 cells in 96-well plates and incubated at 37°C for 7.5 h. Cells subsequently were fixed in 2% formaldehyde (Millipore Sigma) containing 10 μg/mL Hoechst 33342 nuclear stain (Invitrogen) for 45 min at room temperature, when fixative was replaced with PBS. Images were acquired with the InCell 2000 Analyzer (GE Healthcare) automated microscope in both the DAPI and FITC channels to visualize nuclei and infected cells (*i.e.*, eGFP-positive cells), respectively (4X objective, 4 fields per well, covering the entire well). Images were analyzed using the Multi Target Analysis Module of the InCell Analyzer 1000 Workstation Software (GE Healthcare). GFP-positive cells were identified in the FITC channel using the top-hat segmentation method and subsequently counted within the InCell Workstation software. The sensitivity and accuracy of GFP-positive cell number determinations were validated using a serial dilution of virus. A background number of GFP+ cells was subtracted from each well using an average value determined from at least 4 uninfected wells. Data were processed using Prism software (GraphPad Prism 8.0). ACE2 neutralization assays using VSV-SARS-CoV-2-$S_{\Delta 21}$ were conducted similarly but using an MOI of 1. Infection and imaging of Calu-3 cells was performed using similar methods, though cells were infected at an MA104-calculated MOI of 20. Cells were imaged using a 10X objective, with 9 fields per well. FITC and DAPI fields were overlaid using ImageJ and contrast-adjusted identically.

Focus-Reduction Neutralization Test

Indicated dilutions of mAbs, sera, or protein were incubated with 10^2 FFU of SARS-CoV-2 for 1 h at 37°C. Antibody-virus complexes were added to indicated cell monolayers in 96-well plates and incubated at 37°C for 1 h. Subsequently, cells were overlaid with 1% (w/v) methylcellulose in MEM supplemented with 2% FBS. Plates were harvested 30 h later by removing overlays and fixed with 4% paraformaldehyde in PBS for 20 min at room temperature. Plates were washed and sequentially incubated with 1 μg/mL of CR3022 anti-S antibody (ter Meulen et al., 2006; Yuan et al., 2020) and HRP-conjugated goat anti-human IgG in PBS supplemented with 0.1% saponin and 0.1% BSA. SARS-CoV-2-infected cell foci were visualized using TrueBlue peroxidase substrate (KPL) and quantitated on an ImmunoSpot microanalyzer (Cellular Technologies). Data were processed using Prism software (GraphPad Prism 8.0).

QUANTIFICATION AND STATISTICAL ANALYSIS

All statistical tests were performed using GraphPad Prism 8.0 software as described in the indicated figure legends. Statistical significance was assigned when P values were < 0.05. The number of independent experiments and the statistical tests used are indicated in the relevant Figure legends. Error bars indicate standard error of the mean unless stated otherwise.